Advances in Basic and Applied Sciences 6 (2025) 1-13

Advances in Basic and Applied Sciences

journal homepage: https://abas.journals.ekb.eg/

Non-Glacial Origin of the Neoproterozoic Atud Diamictite, Arabian-Nubian Shield: Implications for Pan-African Tectonics and the Snowball Earth Hypothesis

Sayed M. Sayed[1*], Reda Abdu Yousef El-Qassas[2], Amin Esmail Khalil[1], Yahia A. El Kazzaz[1]

[1] *Department of Geology, Faculty of Science, Helwan University, P.O. 11795, Cairo, Egypt*
[2] *Ground Geophysics Department, Exploration Sector, Nuclear Materials Authority (NMA), P.O. Box 530, Maadi, Cairo, Egypt*

ARTICLE INFO

Article history:
Received 8 September 2025
Received in revised form 25 September 2025
Accepted 29 September 2025
Available online 30 September 2025

10.21608/ABAS.2025.421823.1085

Keywords: Atud diamictite, Snowball Earth, Neoproterozoic, Eastern Desert, Molasse sediments, Pan-African orogeny.

Abstract

The Neoproterozoic Atud diamictite of the Central Eastern Desert, Egypt, has long been regarded as a tillite and cited as evidence of glaciation in the Arabian–Nubian Shield. This interpretation, however, rests on data from Wadi Kareim, a correlative section, rather than from the Atud stratotype itself. Here we present new field observations from East of Gabal Atud that challenge the glacial model. The Atud succession is a thick alternation of conglomerates and greywackes, forming distinct fining-upward cycles. Conglomerates are massive, poorly sorted, and exhibit large-scale grading, while greywackes show fining-upward trends, together defining a high-energy depositional system. Sorting is generally poor, and primary sedimentary structures are sparse due to subsequent deformation, yet the overall facies architecture is clear. The diamictite is a coarse, matrix-supported deposit with clasts up to 60 cm in diameter. Petrographic analysis reveals a texturally immature sediment load derived from a diverse suite of igneous, metamorphic, and reworked sedimentary rocks. The deposits lack reliable glacial indicators such as striated pavements, faceted clasts, or lodgement tills, and lack deep-marine features such as turbidites or slumps. Instead, the facies associations are consistent with a Gilbert-type fan-delta/mass flow deposited in a syn-orogenic foreland basin during Pan-African collision. Clast lithologies and published detrital zircon ages indicate mixed sources from juvenile Neoproterozoic arcs and older cratonic crust, signifying continental-scale sediment dispersal during Gondwana assembly. This reinterpretation removes the Atud diamictite as definitive evidence for Cryogenian glaciation in northeast Africa. It highlights the risk of incorporating diamictites into global Snowball Earth compilations without robust type-locality analysis. The Atud succession instead records tectonically driven molasse sedimentation in a foreland basin adjacent to the Pan-African orogen.

* **Corresponding author E-mail:** sayed.mahmoud@science.helwan.edu.eg

1. Introduction

The “Snowball Earth” hypothesis proposes that Earth experienced near-global glaciations during the Cryogenian period (720–635 Ma) [1-7]. A cornerstone of this idea is the widespread occurrence of Neoproterozoic diamictites, many of which have been interpreted as glacial deposits, even at low paleolatitudes [4, 6-9]. Yet “diamictite” is a descriptive, non-genetic term [10, 11], and similar deposits may form by debris flows, olistostromes, or molasse sedimentation in tectonically active basins [12-16]. Distinguishing these origins is critical for paleoclimate reconstruction.

A growing number of classics “tillites” have been reinterpreted as nonglacial. Examples include portions of the Kingston Peak Formation in Death Valley [17, 18], the Kaigas diamictites of southern Africa [19], and parts of the Dwyka and Gowganda successions [20-23], all of which contain extensive mass-flow facies mimicking glacial deposits. These cases highlight that diamictite alone is insufficient to demonstrate glaciation; only integrated sedimentological and stratigraphic analyses can resolve their true origin.

The Atud diamictite of the Eastern Desert of Egypt (Fig.1a) has been widely regarded as evidence for Cryogenian glaciation in the Arabian–Nubian Shield (ANS) [24-27]. Its depositional age of ~750 Ma [25, 28] overlaps with the Sturtian glaciation (~717–660 Ma). However, this interpretation rests on zircon geochronology and observations from Wadi Kareim [24, 25], a correlative unit several kilometers away, rather than from the Atud stratotype itself.

The ANS formed during the Pan-African orogeny (~870–550 Ma), which amalgamated East and West Gondwana through arc collision, ophiolite obduction, and crustal shortening [29-36]. The Central Eastern Desert (Fig.1b), where Atud is exposed, records this tectonic history in stacked thrust sheets of ophiolite, arc volcanics, and syn-orogenic sedimentary basins [34, 37-39]. Such environments are prone to tectonically triggered mass-wasting, producing diamictites that are texturally indistinguishable from glacial deposits.

This study presents a detailed field and petrographic investigation of the Atud diamictite at its type locality east of Gabal Atud. We reassess its depositional setting within the Pan-African tectonic framework and demonstrate that it is best explained as a syn-orogenic molasse succession deposited by high-energy fluvial to alluvial processes. This reinterpretation removes the Atud diamictite as a key pillar of the Snowball Earth hypothesis in the ANS.Instead, it situates it within the foreland basin evolution of the late Neoproterozoic Orogen.

2. Geology of the study area

The Atud Basin (Fig.2) lies within the Central Eastern Desert, the northern sector of the Arabian-Nubian Shield (ANS), a Neoproterozoic accretionary-collisional belt formed during Pan-African orogenesis [33, 34, 36, 40-45].

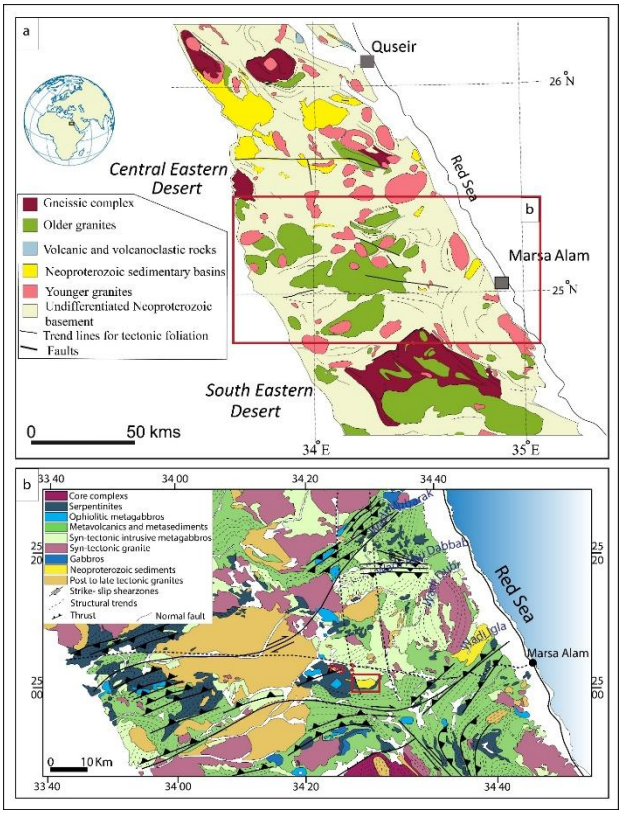

Fig. 1. a) Geological map of the central and southeastern regions of Egypt's Eastern Desert. b) Geological map of the southern part of the Central Eastern Desert of Egypt after [45, 46].

The ANS is characterized by juvenile arc assemblages, ophiolitic remnants, and widespread syn- to post-collisional intrusions; these elements together record protracted arc accretion, ophiolite obduction, and continental collision [34, 36, 43, 47-53]. Tectonism in this setting produces steep relief, rapid unroofing, prolific sediment supply, and frequent slope failure potential [54-62] , all processes capable of generating matrix-supported, polymict deposits that mimic glacial diamictites. Contextualizing the Atud diamictite within this tectonic framework is therefore crucial.

Based on detailed field mapping, the Atud area is composed of four primary, fault-bounded tectono-stratigraphic units [37, 63]. The first is the Metavolcanoclastic schists, which form the structural basement in the south and consist of metamudstones and pebbly schists. The second unit consists of serpentinites, which form a curved thrust sheet that structurally overlie by the Atud sedimentary succession. The third unit is the Atud sedimentary succession, the central unit of investigation, which is a clastic-dominated sequence. Finally, the fourth unit is the igneous intrusive complex, a multi-phase suite of gabbro, tonalite, and granodiorite that

* **Corresponding author E-mail:** sayed.mahmoud@science.helwan.edu.eg

intrudes the Atud sedimentary succession [63], with U-Pb zircon ages of ~695 Ma placing it firmly in the syn-orogenic period [64]. Field observation indicates that the contacts between these major units are tectonic, defined by shear zones and thrust faults, pointing to a highly active and compressional tectonic regime during and after deposition.

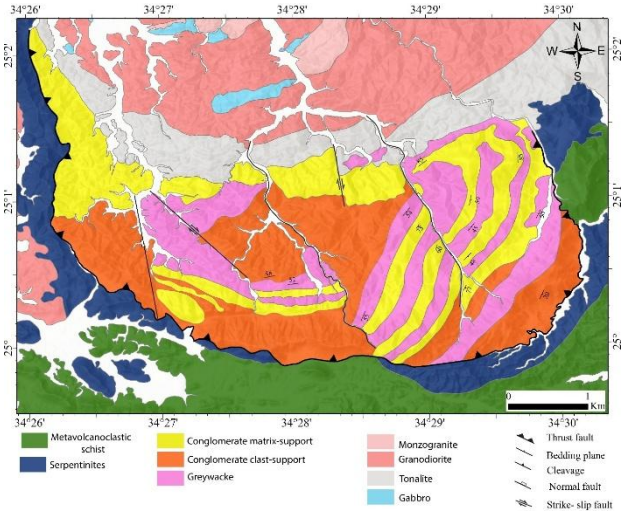

Fig. 2. A geological map illustrating the tectono-stratigraphic units of the Atud basin and the differentiated igneous bodies of the gabbro-tonalite-granodiorite complex after [63].

The detrital zircon data of the Atud sedimentary succession [28] reveal a composite age spectrum dominated by Neoproterozoic populations, minor early Neoproterozoic grains, and a significant older component of Paleoproterozoic to Archean zircons. The youngest coherent Neoproterozoic populations indicate a maximum depositional age near ~720± 20 Ma, placing deposition within the Sturtian interval. However, the mixed and recycled nature of older populations demonstrates sediment routing from both juvenile ANS terranes and older cratonic sources, consistent with a continental-scale sediment dispersal system operating during Pan-African assembly. Interpreting these age spectra in isolation as evidence for glaciation is unreliable; instead, they support an origin tied to active orogen erosion and recycling.

3. Methodology

This study integrates detailed field observations, petrographic analysis, and published detrital zircon geochronology, to evaluate the origin of the Atud diamictite.

3.1 Fieldwork and Sampling

Comprehensive field mapping was conducted across the Atud Basin, with particular focus on the diamictite successions. Structural orientations, clast characteristics (size, shape, lithology, and fabric), and depositional relationships with adjacent units were systematically documented. Representative samples of diamictite and associated lithologies were collected for petrographic analysis.

3.2 Petrographic Analysis

Representative clasts and matrix samples were cut and prepared as standard 30-micron thin sections for transmitted-light petrography. Modal composition, grain textures, and alteration features were described to classify clast lithologies and to assess provenance. Particular attention was given to distinguishing between plutonic, volcanic, sedimentary, and metamorphic components.

3.2. Detrital Zircon U–Pb Geochronology

Provenance constraints were obtained from published U–Pb ages by Li, Abd El-Rahman [28] of detrital zircons from the Atud Formation greywackes and associated volcanic clasts. These data were re-evaluated in the context of field and petrographic observations to establish source regions and sediment dispersal pathways. The combined dataset was used to critically evaluate competing models for the origin of the Atud diamictite. Textural evidence, provenance signals, and structural context were synthesized to distinguish between a glacial versus tectonic mass-flow origin.

4. Results

4.1 The Atud Sedimentary Succession: Field-Based Lithofacies Analysis

Field investigation of the Atud succession reveals three principal, interbedded lithological packages. The nature and relationship of these facies provide crucial evidence regarding the depositional environment. Greywackes represent the predominant lithology within succession and are frequently interbedded with the conglomerate units. Many greywacke outcrops exhibit intense cleavage development (Fig. 3a), a clear field indicator of significant strain. The second package, the matrix-supported conglomerate, is the focus of the debate. Field observations show a chaotic, poorly sorted deposit where clasts ranging from 30 cm to 60 cm in size are supported by a sand-sized matrix. The clasts are polymictic and vary in shape from angular (Fig. 3b) to rounded (Fig.3c, d) to ovoidal (Fig.3e) to elliptical (Fig.3f). The matrix of this diamictite is not pristine; in many outcrops, it displays a high degree of cleavage with a consistent E-W strike (Fig.3g), indicating it has undergone significant tectonic shortening.

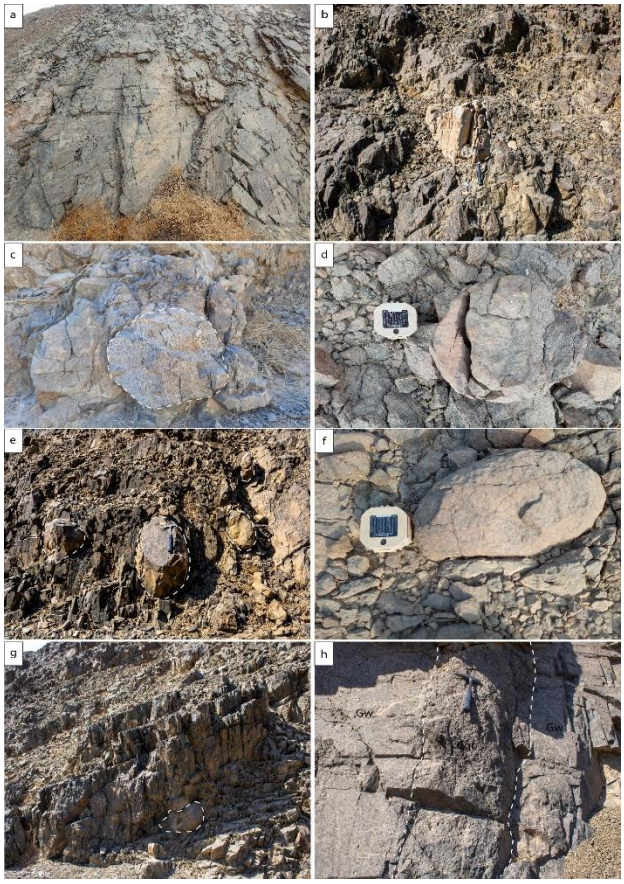

Fig. 3. Field photographs of the Atud diamictite. a) highly cleavage greywacke (Looking N; GPS: 25° 0'47.40"N, 34°28'0.10"E); b) Angular marble boulder embedded within the diamictite matrix (looking SW; GPS: 25° 1'3.83"N, 34°28'53.25"E); c) Rounded granite cobble in the diamictite (looking E; 25° 1'0.31"N, 34°28'56.27"E); d) Rounded greywacke cobble in the diamictite (looking S; GPS: 25° 0'44.72"N, 34°28'2.75"E); e) oval boulders of greywacke within the Atud diamictite (looking toward the W; GPS: 25° 1'4.08"N, 34°28'52.96"E); f) elliptical greywacke clasts (looking WSW; GPS: 25° 0'44.84"N, 34°28'2.86"E); g) Intensely penetrative E–W cleavage in diamictite outcrop (looking SWS; GPS: 25° 1'4.17"N, 34°28'52.95"E); and h) conglomerate clast support interbedded with greywacke (looking E; GPS: 25° 0'27.30"N , 34°29'17.67"E).

The third package is the clast-supported conglomerate, which consists of coarse-grained, better-sorted beds composed of rounded, polymictic pebbles in grain-to-grain contact (Fig.3h). The intimate interbedding of these three facies is the classic signature observed in proximal Gilbert-type delta built at the foot of a rapidly uplifting tectonic source area.

The structural setting of the Atud Basin, as observed in the field, is fundamentally inconsistent with deposition in a passive, glacially influenced environment. Instead, it points directly to a syn-tectonic origin within a compressional orogen. The succession is tectonically bounded, thrust over serpentinites and metavolcanoclastic schists along major faults. Internally, the basin is deformed by a series of E-W striking thrusts and a large-scale, NE-SW trending anticline. These structures indicate that the basin was subjected to significant crustal shortening. These field observations collectively demonstrate that the Atud Basin was not a quiescent depocenter but was actively deforming within a compressional orogen during and immediately after sedimentation.

4.2 Petrography of Clasts in the Atud Diamictite

Petrographic analysis of the Atud diamictite reveals a polymictic clast assemblage derived from diverse lithologies. Igneous components include felsite, quartz porphyry, and granite porphyry, while sedimentary clasts consist mainly of greywacke and quartz arenite. Metamorphic fragments are also present, dominated by marble with rare mica schist. This wide spectrum of plutonic, volcanic, sedimentary, and metamorphic sources points to rapid unroofing of multiple crustal levels, consistent with provenance from an actively uplifting collisional orogen.

4.2.1 Igneous Pebble Assemblage

4.2.1.1 Granitic Pebbles

Granitic pebbles are less frequent but petrographically distinctive. They are generally rounded to subrounded, equidimensional, and display a hypidiomorphic texture. Macroscopically, they show pinkish to greenish-grey colors and medium to coarse grain sizes. Biotite, euhedral plagioclase, and interstitial quartz dominate the mineralogy. Under the microscope, quartz grains (up to 2 mm) exhibit undulose extinction (Fig. 4a). Plagioclase crystals show sericitization and contain calcite inclusions. Biotite, frequently altered to chlorite, is intergrown with accessory rutile, and iron oxides.

4.2.1.2 Volcanic Pebbles

4.2.1.2.1 Felsite

Felsite pebbles are fine-grained, grey to greenish rocks with phenocrysts of quartz, sanidine, and plagioclase within a microlitic groundmass. Quartz shows resorption textures (Fig.4b). Sanidine and plagioclase phenocrysts exhibit twinning and are often altered to sericite or kaolinite. Biotite, partially chloritized, is associated with rutile sagenitic textures.

4.2.1.2.2 Quartz Porphyries

Quartz porphyry clasts exhibit prominent phenocrysts of quartz (Fig. 4c), which are strained, fractured, and

partially resorbed. The groundmass includes feldspars and biotite, often aligned to produce directive textures. Plagioclase is partially sericitized and includes calcite and dusty inclusions.

4.2.1.2.3 Granite Porphyries

Granite porphyry pebbles are rare and identified by pink to greenish hues. They contain large plagioclase phenocrysts (Fig. 4d) with complex twinning and inclusions. Quartz and orthoclase in the groundmass exhibit mosaic and microperthitic textures. Biotite is pleochroic and often corroded by feldspar.

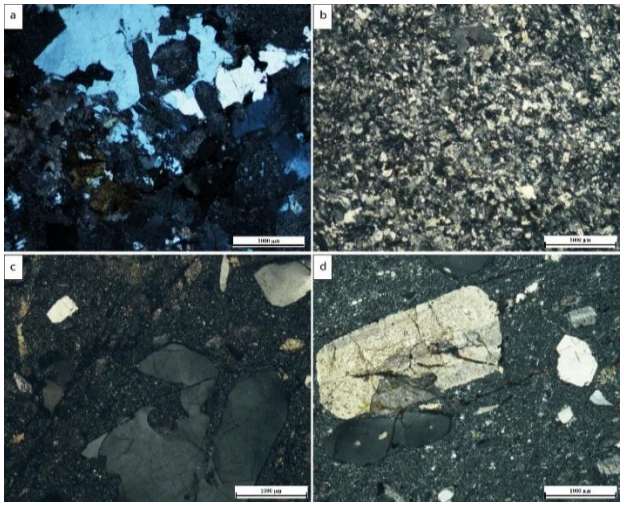

Fig. 4. Photomicrographs of igneous clasts from the Atud conglomerate (XPL). a) Granite with strained quartz, sericitized plagioclase, and chloritized biotite; b) Felsite with quartz–feldspar phenocrysts in fine groundmass, biotite altered to chlorite/calcite; c) Quartz porphyry with embayed quartz phenocrysts in cryptocrystalline feldspar–biotite matrix; and d) Granite porphyry with sericitized plagioclase and quartz inclusions in quartz–orthoclase groundmass, altered pleochroic biotite.

4.2.2 Reworked Sedimentary Pebbles

4.2.2.1 Greywacke

Greywacke pebbles are the most common and often ellipsoidal with flat alignment. These fine-grained, grey rocks consist mainly of (Fig. 5a) quartz and feldspar embedded in a fine matrix of biotite, chlorite, and iron oxides. Quartz grains exhibit anhedral shape. Plagioclase grains show mild alteration to sericite.

4.2.2.2 Quartz Arenites

Quartz arenites are well-washed, sorted equivalents of greywackes, dominated by quartz and feldspar with minor muscovite and epidote. Grains are subrounded (Fig. 5b), often showing secondary quartz overgrowths. Feldspars are typically altered, with plagioclase showing kaolinitization.

4.2.3 Metamorphic Pebbles

4.2.3.1 Marble Pebbles

Marble pebbles are abundant and display fine-grained calcite mosaics with occasional color variation (grey to greenish-pink). Under the microscope, they show anhedral calcite (0.2–0.7 mm) interlocked without voids (Fig. 5c). Veinlets of calcite crosscut the texture (Fig. 5d). Some slices display sandy-marble interbands rich in quartz and mica (Fig. 5e). Banded marbles exhibit alternating layers of pure calcite and mixed sandy-calcareous material, indicating sedimentary reworking of older metamorphic rocks.

4.2.3.2 Mica Schists

Mica schist fragments are rare components within the Atud conglomerate and are primarily composed of quartz, sericite, biotite, and chlorite, with minor feldspar and accessory iron oxides (Fig. 5f). The rock displays a well-developed schistose texture, characterized by the parallel alignment of platy minerals. Sericite appears fine, colorless, and typically unbent shreds. Biotite occurs as minute, honey-brown flakes, while chlorite is present as olive-green plates showing anomalous blue interference colors under cross-polarized light. Quartz forms fine-grained, anhedral crystals dispersed throughout the matrix. This mineralogical assemblage and texture reflect low- to medium-grade regional metamorphism.

5. Discussion

5.2 Provenance of the Atud Diamictite

Provenance analysis integrates our field and petrographic observations with the published detrital zircon dataset of Li et al., 2018, which we correlate with exposed source terranes. The Atud diamictite at the type locality is a polymict assemblage of clasts up to 50 cm in diameter set in a greywacke matrix, including granitoid, quartz porphyry, quartzite, marble, basalt, arkose, and intraformational greywacke and marble. Thin-section study confirms contributions from plutonic, volcanic, sedimentary, and metamorphic sources, and field fabrics such as preferred clast orientation and abundant intraformational fragments indicate rapid erosion, short transport distances, and high-energy mass-flow deposition.

When mapped onto the Li et al., 2018 zircon-age spectrum, these lithological observations refine the sediment-routing model for the Atud Basin. The dominant Neoproterozoic population, broadly 740–870 Ma, is represented by euhedral to subhedral grains, which is

consistent with short transport from nearby juvenile arc terranes that were actively unroofing during deposition.

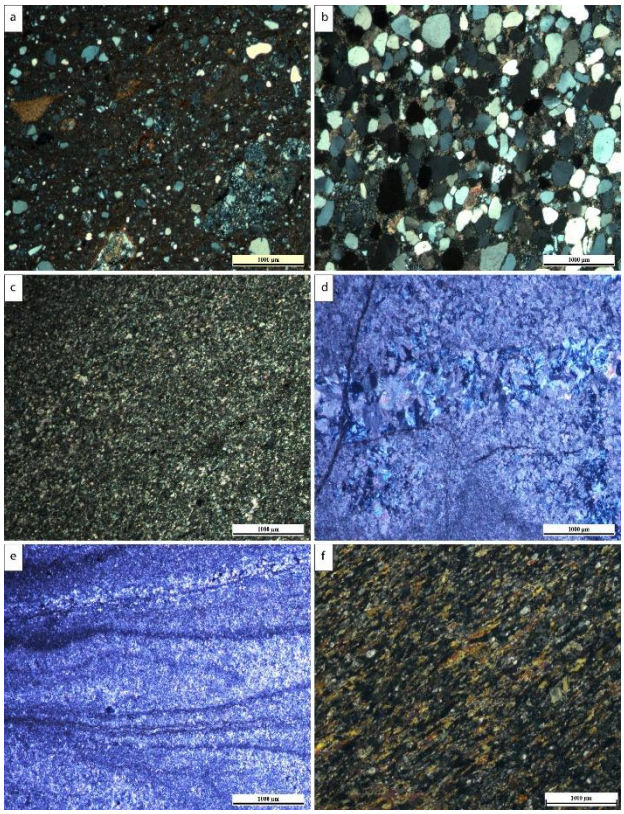

Fig. 5. Photomicrographs of sedimentary and metamorphic clasts from the Atud conglomerate (XPL). a) Greywacke with fine quartz and feldspar in a micaceous matrix, weak schistosity; b) Quartz arenite with rounded quartz grains showing overgrowths and kaolinized feldspar; c) Marble of interlocking calcite with minor quartz and muscovite; d) Calcite veinlets crosscutting marble; e) Sandy–marble interbands rich in quartz and mica; and f) Mica schist with aligned sericite, biotite, and chlorite, and interstitial anhedral quartz.

We correlate these ages with exposed arc and plutonic terranes in the region, including Wadi Beitan ~719–725 Ma [65], the Asir terrane 800–700 Ma [66], the Haya terrane 830–720 Ma [67], and the Jiddah terrane 870–760 [34]. A subordinate early Neoproterozoic component (~902–930 Ma) likely reflects recycling of older arc crust incorporated into the collisional orogen [28].

A significant Paleoproterozoic to Archean population (c. 1.75–2.85 Ga), dominated by rounded grains, points to distal cratonic inputs, most plausibly from the Saharan Metacraton and allied East Gondwana fragments [68-71]. Notably, the Li et al., 2018 dataset shows an absence of Mesoproterozoic ages (1.0–1.7 Ga), a pattern that is regionally characteristic of the Arabian–Nubian Shield and which further constrains possible source areas. By combining the Li et al., 2018 age spectra with direct clast petrography (Table 1), we demonstrate that the Atud Basin received simultaneous input from nearby Pan-African arcs, recycled Neoproterozoic crust, and more distant cratonic blocks. This mixed provenance, together with the field evidence for rapid, high-energy deposition, is most consistent with syn-orogenic molasse sedimentation in a foreland basin, and it does not require glacial transport mechanisms.

5.2 Origin of the Atud Diamictite: Syn-orogenic Molasse vs. Glacial Deposition

The Atud diamictite has been repeatedly cited as a Cryogenian tillite, but observations at its type locality show features inconsistent with glacial deposition. Classic syntheses proposed multiple discrete glacial episodes, sometimes as many as four [4, 7, 24], tied to Rodinia rifting and evolving basin configurations, while others argued for three [72]. By contrast, several analyses distilled the record to two globally synchronous events, the Sturtian (~717–660 Ma) and Marinoan (~651–635 Ma) glaciations [1, 6, 73, 74] This lack of consensus, spanning tectonic alternatives such as Eyles and Januszczak [13] “zipper-rift” model to high-precision U–Pb geochronology converging on two events [9], underscores the risks of assigning all Cryogenian diamictites to direct glacial origins.

Moreover, classic Snowball Earth “indicators” are similarly ambiguous. Banded iron formations (BIFs), raised as markers of deglacial oxygenation, are also found within volcanic arcs and restricted basins, with geochemical signatures pointing to hydrothermal input and microbial mediation [39, 75-77]. Cap carbonates, long considered diagnostic of postglacial flooding, are likewise non-unique, shaped by ocean chemistry, productivity, and diagenesis [4, 24, 73, 74, 78-80]. In the Atud Basin, systematic fieldwork revealed no preserved cap carbonates, eliminating a key expectation of a Snowball Earth succession. Direct sedimentological evidence of glacial transport is also absent. No striated pavements, faceted clasts, bullet-shaped clasts, or iceberg-rafted outsized blocks deforming underlying laminae were identified despite targeted searches across multiple exposures. The absence of these reliable ice-grounding indicators significantly undermines the glacial model [12, 15, 22, 81-83]. Similar reappraisals have shifted interpretations of other classic Cryogenian units, such as the Kingston Peak Formation in Death Valley [17, 18], the Kaigas diamictites in Namibia and South Africa [19], and even the Paleoproterozoic Gowganda Formation of Canada [15, 23], from glacial to nonglacial origins.

Table 1. Provenance synthesis: detrital-zircon age peaks Li, Abd El-Rahman [28] correlated with exposed terranes and Atud field evidence

Age range	Representative zircons	Correlative terrane (exposed units)	Field evidence (Atud type locality)	Citation
~740–870 Ma (Neoproterozoic)	Euhedral to subhedral, coherent youngest populations, high abundance	Juvenile Pan-African arc and plutonic terranes: Wadi Beitan (~719–725 Ma), Asir (800–700 Ma), Haya (830–720 Ma), Jiddah (870–760 Ma)	Dominant age group in Li et al., 2018, consistent with short transport, abundant volcanic and plutonic clasts (felsite, quartz porphyry, granite porphyry), large polymict clasts up to 50–60 cm, preferred clast orientation indicating proximal sourcing.	Li et al., 2018; Ali et al., 2015; Camp, 1984; Abdelsalam and Stern, 1993; Hamimi et al., 2022.
~902–930 Ma (early Neoproterozoic, minor population)	Subrounded to subhedral grains, subordinate population	Recycled early Neoproterozoic arc crust, older arc remnants incorporated into the orogen	Minor population in Li et al., 2018, matches field evidence for reworked arc-derived clasts and textural evidence for recycling (intraformational greywacke fragments).	Li et al., 2018; regional arc studies.
~1.75–2.85 Ga (Paleoproterozoic to Archean)	Predominantly rounded grains, indicating long transport/recycling	Cratonic sources, e.g., Saharan Metacraton, possible East Gondwana fragments	Rounded ancient zircons in Li et al., 2018, paired with presence of Paleoproterozoic–Archean clast lithologies (marble, quartzite) in the Atud assemblage, indicating distal supply and long sediment-routing.	Li et al., 2018; Dixon, 1981; Abdelsalam et al., 2003; Johnson et al., 2011; Meinhold et al., 2020.
1.0–1.7 Ga (Mesoproterozoic)	—	Not represented	Absence noted in Li et al., 2018, consistent with regional ANS detrital-zircon patterns, helps exclude Mesoproterozoic source provinces.	Li et al., 2018; regional syntheses.

In contrast, the Atud diamictite shows features consistent with syn-orogenic molasse sedimentation. The succession is composed of cyclic greywacke-conglomerate alternations with clasts up to 60 cm derived from nearby Precambrian basement , deposited in a high-energy fluvial to alluvial environment [63]. Such features are typical of foreland basins adjacent to active orogens, where rapid uplift supplies polymictic detritus and coseismic slope failures generate mass-wasting events (Fig. 6) [6, 12, 13, 21, 82, 84, 85]. Syn-depositional deformation, cleavage development, and the tectonic context of arc collision and ophiolite obduction between 820 and 660 Ma [36] reinforce this interpretation.

Correlative successions in northern Ethiopia, temporally linked to Atud, show positive $\delta^{13}C$ excursions (+7 ‰) in shallow-marine carbonates rather than the isotopic collapse expected under global glaciation [86, 87]. Together, these data point to tectonically driven molasse deposition in a foreland basin during the Pan-African orogeny.

The Atud diamictite thus exemplifies the broader "diamictite conundrum": without unambiguous glacial indicators, diamictites cannot be treated as definitive climate archives. Instead, the Atud succession records a tectono-sedimentary response to Pan-African Mountain building rather than grounded ice.

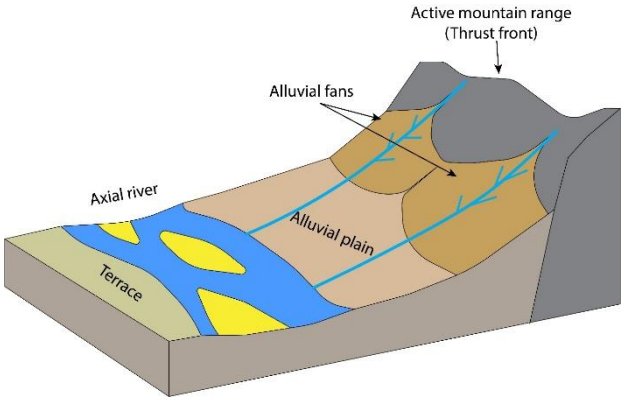

Fig. 6. Depositional setting and paleoenvironment adjacent to thrust front after [88-90]

5.2 The Wadi Kareim Formation and Its Distinction from Atud

Ali, Stern [25] described the Atud diamictite at Wadi Kareim as a poorly sorted, matrix-supported polymictic breccia, with clasts up to one meter in size and lithologies ranging from granitoid and quartz porphyry to greywacke, marble, and basalt, and highlighted the stratigraphic association with banded iron formation (BIF). On this basis, they proposed that the Atud diamictite was a Cryogenian glacial deposit.

However, this description corresponds closely to the

* **Corresponding author E-mail:** sayed.mahmoud@science.helwan.edu.eg

general sedimentary and volcanic succession of the Wadi Kareim Basin, which is known to contain volcanogenic greywackes, conglomerates, arc volcanic rocks, with association of BIF [35, 91, 92]. The clast types and facies Ali et al. list are consistent with the basin's local volcanic and plutonic sources and are not unique to the Atud succession. Furthermore, the stratigraphic association between BIF and matrix-supported conglomerates is unique to Wadi Kareim and does not occur at the Atud type locality [24, 25, 70].

During our own fieldwork, we revisited the Wadi Kareim exposures that Ali et al. (2010) identified as Atud diamictite. We observed that the clasts there are markedly smaller and less variable in size compared with those at the Atud type section. More significantly, the matrix in these Kareim deposits is pervasively sheared, in contrast to the Atud diamictite where the matrix lacks such penetrative shear fabric. This difference is critical: the sheared matrix at Kareim reflects deformation within the volcano-sedimentary succession of the Kareim Basin, not primary depositional features of the Atud diamictite.

These field observations, supported by photographs (Fig. 7), demonstrate that the lithology at Wadi Kareim differs from the Atud succession. The use of Kareim Basin sediments as a direct analogue for the Atud diamictite is therefore problematic. Ali et al.'s description appears to reflect local facies of the Kareim Basin, rather than the Atud type locality itself, and conflating the two has introduced interpretive bias into the glacial versus nonglacial debate.

Conclusion

Field, petrographic and provenance data from the Atud type locality indicate that the Atud diamictite is best interpreted as a syn-orogenic, tectono-sedimentary deposit rather than a primary glacial till. The main conclusions are:

1. Sedimentary and structural character: The succession comprises abundant polymict clasts, locally 50–60 cm in diameter, set in a greywacke matrix, shows preferred clast orientations and intraformational recycling, and is overprinted by a pervasive penetrative cleavage within a thrust-bounded basin architecture. These attributes are consistent with high-energy mass-flow and molasse processes adjacent to an actively uplifting orogen, not with deposition by grounded ice.
2. Provenance: Re-evaluation and correlation of the published detrital-zircon dataset (Li et al., 2018) with exposed source terranes shows a dominant Neoproterozoic signal (c. 740–870 Ma), subordinate early Neoproterozoic ages (c. 902–930 Ma), and a significant Paleoproterozoic to Archean component (c. 1.75–2.85 Ga). Zircon textures and the clast assemblage indicate short transport from juvenile Pan-African arc and plutonic sources, with recycled and distal cratonic input, a provenance pattern expected for syn-orogenic molasse in a foreland setting.

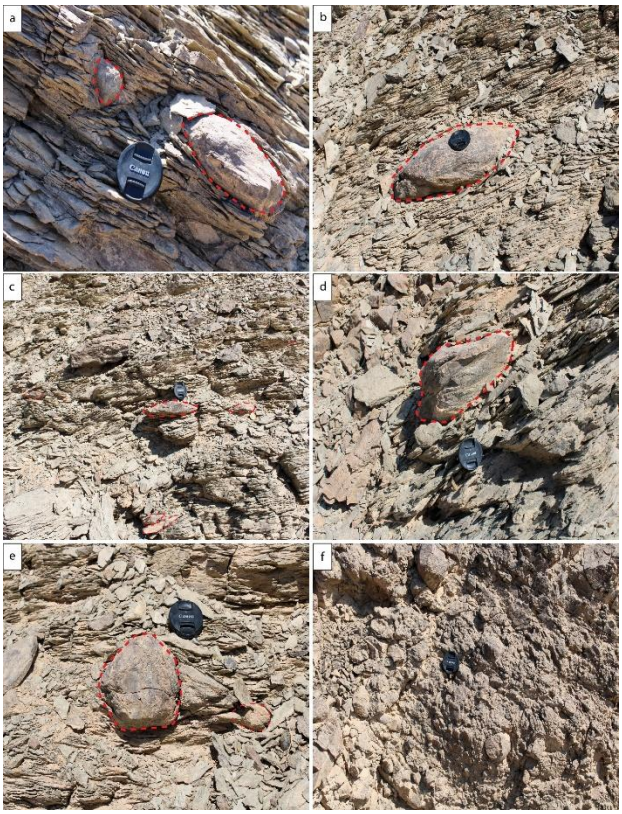

Fig. 7. Field photographs of the Wadi Kareim what is called diamictite, illustrating clast characteristics and matrix fabric. (a) Oval pebbles and boulders enclosed within a pervasively sheared matrix (looking NE; GPS: 25°57'3.45"N, 34° 1'41.45"E. (b) Elliptical clast aligned within the sheared matrix (looking NE; GPS: 25°57'3.96"N, 34° 1'41.89"E). (c) Pebbles with long axes preferentially oriented parallel to bedding (looking NE; GPS: 25°57'3.96"N, 34° 1'41.89"E). (d) Large oval boulder set within the matrix (looking NE; GPS:25°57'5.90"N, 34° 1'42.73"E). (e) Rounded to subrounded cobbles typical of the Kareim facies (looking NE; GPS:25°57'5.85"N, 34° 1'42.75"E). (f) Clast-supported conglomerate exposure from Wadi Kareim (looking NNE; GPS:25°57'4.64"N, 34° 1'42.77"E).

3. Miscorrelation with Wadi Kareim: The prior assignment of Atud to Cryogenian glaciation relied heavily on correlative exposures at Wadi Kareim (Ali et al., 2010). Our field revisits show

the Kareim deposits differ from the Atud stratotype in clast size distributions and matrix fabric, the latter being pervasively sheared at Kareim but not at Atud (see Fig. 6). Therefore, the Kareim description reflects local basin facies and should not be conflated with diagnostic features of the Atud type section.

4. Implications for Cryogenian records: Given the lack of unequivocal ice-grounding indicators at the type locality, Atud should not be treated as a robust Cryogenian glacial datum in regional Snowball Earth compilations until independent, multi-proxy glacial evidence is demonstrated.
5. Tectonic significance: The Atud succession more appropriately documents the sedimentary response to Pan-African tectonism, recording rapid uplift, unroofing and high-flux sediment delivery into a thrust-bounded basin during Gondwana assembly.

In summary, the Atud diamictite exemplifies the diamictite conundrum: in the absence of unequivocal, multi-proxy glacial indicators, diamictites remain ambiguous. For Atud, the balance of evidence favours a tectonic, syn-orogenic origin rather than a glacial one.

Future work

To remove remaining ambiguities and to tighten age constraints we recommend: (a) high-precision CA-ID-TIMS dating of the youngest detrital zircons; (b) systematic paleocurrent and fabric analyses to quantify transport directions and flow regimes.

Ethics approval

Not applicable.

Availability of data and material

Avaliable upon request.

Conflict of interest

The author declared no potential conflicts of interest concerning this article's research, authorship, and publication.

Funding

The author received no financial support for the research.

Acknowledgment

The author thanks anonymous reviewers for their comments that enhance the paper's present form.

References

1. Kennedy, M., *Two or four Neoproterozoic glaciations?* Geology, 1998. **26**: p. 1059-1063.
2. Hoffman, P.F., et al., *A Neoproterozoic Snowball Earth.* Science, 1998. **281**(5381): p. 1342-1346.
3. Hoffman, P., *Hoffman, P. F. On Cryogenian (Neoproterozoic) ice-sheet dynamics and the limitations of the glacial sedimentary record. 28th DeBeers Alexander Du Toit Memorial Lecture. S. Afr. J. Geol. 108, 557-576.* South African Journal of Geology - S AFR J GEOL, 2005. **108**: p. 557-577.
4. Hoffman, P.F. and D.P. Schrag, *The snowball Earth hypothesis: testing the limits of global change.* Terra Nova, 2002. **14**(3): p. 129-155.
5. Hoffman, P.F., *The break-up of Rodinia, birth of Gondwana, true polar wander and the snowball Earth.* Journal of African Earth Sciences, 1999. **28**(1): p. 17-33.
6. Allen, P.A. and J.L. Etienne, *Sedimentary challenge to Snowball Earth.* Nature Geoscience, 2008. **1**(12): p. 817-825.
7. Evans, D., *Stratigraphic, geochronological, and paleomagnetic constraits upon the Neoproterozoic climatic paradox.* American Journal of Science - AMER J SCI, 2000. **300**: p. 347-433.
8. Macdonald, F.A., et al., *Calibrating the Cryogenian.* Science, 2010. **327**(5970): p. 1241-1243.
9. Cox, G.M., et al., *South Australian U-Pb zircon (CA-ID-TIMS) age supports globally synchronous Sturtian deglaciation.* Precambrian Research, 2018. **315**: p. 257-263.
10. Flint, R.F., J.E. Sanders, and J. Rodgers, *SYMMICTITE: A NAME FOR NONSORTED TERRIGENOUS SEDIMENTARY ROCKS THAT CONTAIN A WIDE RANGE OF PARTICLE SIZES.* GSA Bulletin, 1960b. **71**(4): p. 507-510.
11. Flint, R.F., J.E. Sanders, and J. Rodgers, *DIAMICTITE, A SUBSTITUTE TERM FOR SYMMICTITE.* GSA Bulletin, 1960a. **71**(12): p. 1809-1810.
12. Jensen, P.A. and E. Wulff-Pedersen, *Glacial or non-glacial origin for the Bigganjargga tillite,*

Finnmark, northern Norway. Geological Magazine, 1996. **133**(2): p. 137-145.
13. Eyles, N. and N. Januszczak, *'Zipper-rift': a tectonic model for Neoproterozoic glaciations during the breakup of Rodinia after 750 Ma.* Earth-Science Reviews, 2004. **65**(1): p. 1-73.
14. Vesely, F.F., et al., *Recurrent emplacement of non-glacial diamictite during the late Paleozoic ice age.* Geology, 2018. **46**(7): p. 615-618.
15. Molén, M.O., *Field evidence suggests that the Palaeoproterozoic Gowganda Formation in Canada is non-glacial in origin.* Geologos, 2021. **27**: p. 73 - 91.
16. Khan, M.M.S.S., et al., *A newly discovered Neoproterozoic diamictite-cap carbonate couplet from the Western Himalaya: The expansion of the Marinoan snowball Earth glaciation to the northwestern margin of the Indian Plate in North Pakistan.* Precambrian Research, 2022. **378**: p. 106759.
17. Le Heron, D.P., et al., *A diamictite dichotomy: Glacial conveyor belts and olistostromes in the Neoproterozoic of Death Valley, California, USA.* Geology, 2017. **45**(1): p. 31-34.
18. Tofaif, S., et al., *Glaciers, flows, and fans: Origins of a Neoproterozoic diamictite in the Saratoga Hills, Death Valley, California.* Sedimentary Geology, 2019. **385**: p. 79-95.
19. Pu, J.P., et al., *Tonian basins record rifting of Kalahari from Rodinia and no evidence of a pre-Sturtian Kaigas glaciation.* Earth and Planetary Science Letters, 2023. **624**: p. 118472.
20. Herbert, C.T. and J.S. Compton, *Depositional environments of the lower Permian Dwyka diamictite and Prince Albert shale inferred from the geochemistry of early diagenetic concretions, southwest Karoo Basin, South Africa.* Sedimentary Geology, 2007. **194**(3): p. 263-277.
21. Molen, M., *Field evidence suggests that the Palaeoproterozoic Gowganda Formation in Canada is non-glacial in origin.* Geologos, 2021. **27**: p. 73-91.
22. Molen, M. and J. Smit, *Reconsidering the glaciogenic origin of Gondwana diamictites of the Dwyka Group, South Africa.* Geologos, 2022. **28**: p. 83–113.
23. Kennedy, K. and N. Eyles, *The Paleoproterozoic (c. 2.3 Ga) Gowganda Formation: Deep water, glacially-influenced debrites and related mass flow along a passive margin.* Earth-Science Reviews, 2025. **261**: p. 105033.
24. Stern, R.J., et al., *Evidence for the Snowball Earth hypothesis in the Arabian-Nubian Shield and the East African Orogen.* Journal of African Earth Sciences, 2006. **44**(1): p. 1-20.
25. Ali, K., et al., *Neoproterozoic diamictite in the Eastern Desert of Egypt and Northern Saudi Arabia: Evidence of ~750 Ma glaciation in the Arabian-Nubian Shield?* International Journal of Earth Sciences, 2010. **99**: p. 705-726.
26. Stern, R.J., et al., *Chapter 22 Evidence for Early and Mid-Cryogenian glaciation in the Northern Arabian–Nubian Shield (Egypt, Sudan, and western Arabia).* Geological Society, London, Memoirs, 2011. **36**(1): p. 277-284.
27. Miller, N. and B. Stern, *Evolution of the Arabian Nubian Shield and Snowball Earth*. 2021. p. 153-194.
28. Li, X.-H., et al., *Old Continental Crust Underlying Juvenile Oceanic Arc: Evidence From Northern Arabian-Nubian Shield, Egypt.* Geophysical Research Letters, 2018. **45**(7): p. 3001-3008.
29. Stern, R.J., *ARC ASSEMBLY AND CONTINENTAL COLLISION IN THE NEOPROTEROZOIC EAST AFRICAN OROGEN: Implications for the Consolidation of Gondwanaland.* Annual Review of Earth and Planetary Sciences, 1994. **22**(Volume 22, 1994): p. 319-351.
30. Kröner, A. and B. Stern, *Pan-African Orogeny*. 2004. p. 1-12.
31. Collins, A.S. and B.F. Windley, *The tectonic evolution of central and northern Madagascar and its place in the final assembly of Gondwana.* The Journal of geology, 2002. **110**(3): p. 325-339.
32. Cawood, P.A., et al., *Accretionary orogens through Earth history.* Geological Society, London, Special Publications, 2009. **318**(1): p. 1-36.
33. Hamimi, Z., et al., *Large-scale geological structures of the Egyptian Nubian Shield.* Scientific Reports, 2023. **13**: p. 1-15.
34. Hamimi, Z., et al., *The Tectonic Map and Structural Provinces of the Late Neoproterozoic Egyptian Nubian Shield: Implications for Crustal Growth of the Arabian–Nubian Shield (East African Orogen).* Frontiers in Earth Science, 2022. **10**.
35. Fowler, A.-R. and Z. Hamimi, *Post-amalgamation Depositional Basins in the Arabian-Nubian Shield: The Hammamat Basins of Egypt*, in *The Geology of the Arabian-Nubian*

Shield, Z. Hamimi, et al., Editors. 2021, Springer International Publishing: Cham. p. 451-483.
36. Abd El-Wahed, M. and Z. Hamimi, *Neoproterozoic Tectonic Events of Egypt.* Acta Geologica Sinica - English Edition, 2021. **95**(4): p. 1366-1405.
37. Akaad, M. and M. Essawy, *Geology and structure of the area east of Gabal Atud, Eastern Desert of Egypt.* Bulletin of Science and Technology, 1964. **7**: p. 75-102.
38. Fawzy, M.M., N.M. Mahdy, and M. Sami, *Mineralogical characterization and physical upgrading of radioactive and rare metal minerals from Wadi Al-Baroud granitic pegmatite at the Central Eastern Desert of Egypt.* Arabian Journal of Geosciences, 2020. **13**: p. 1-15.
39. Sami, M., et al., *Unravelling the genesis and depositional setting of Neoproterozoic banded iron formation from central Eastern Desert, Egypt.* Frontiers in Earth Science, 2024. **Volume 12 - 2024**.
40. Hamimi, Z., et al., *Tectonics of the Eastern Desert of Egypt: Key to Understanding the Neoproterozoic Evolution of the Arabian–Nubian Shield (East African Orogen)*. 2019.
41. Fowler, A.-R. and Z. Hamimi, *Structural and tectonic framework of Neoproterozoic basement of Egypt: from gneiss domes to transpression belts*, in *The geology of Egypt*. 2019, Springer. p. 81-129.
42. El-Bialy, M.Z., *Precambrian Basement Complex of Egypt*, in *The Geology of Egypt*, Z. Hamimi, et al., Editors. 2020, Springer International Publishing: Cham. p. 37-79.
43. Osman, A.F. and A.-R. Fowler, *Terrane Accretion Within the Arabian-Nubian Shield*, in *The Geology of the Arabian-Nubian Shield*, Z. Hamimi, et al., Editors. 2021, Springer International Publishing: Cham. p. 221-266.
44. Abd El-Wahed, M., *Thrusting and transpressional shearing in the Pan-African nappe southwest El-Sibai core complex, Central Eastern Desert, Egypt.* Journal of African Earth Sciences, 2008: p. 16-36.
45. Abd El-Wahed, M.A., *Oppositely dipping thrusts and transpressional imbricate zone in the Central Eastern Desert of Egypt.* Journal of African Earth Sciences, 2014. **100**: p. 42-59.
46. Abd El-Wahed, M.A., H. Harraz, and M.H. El-Behairy, *Transpressional imbricate thrust zones controlling gold mineralization in the Central Eastern Desert of Egypt.* Ore Geology Reviews, 2016. **78**: p. 424-446.
47. El-Bialy, M.Z., et al., *Continental Arc Plutonism in a Juvenile Crust: The Neoproterozoic Metagabbro-Diorite Complexes of Sinai, Northern Arabian-Nubian Shield.* Minerals, 2024. **14**(2): p. 145.
48. Ali, S., M.K. Azer, and A.-A.M. Abdel-Karim, *Origin and evolution of Neoproterozoic metaophiolitic mantle rocks from the eastern Desert of Egypt: Implications for tectonic and metamorphic events in the Arabian-Nubian Shield.* Geologica Acta, 2023.
49. Peng, P., et al., *Cryogenian accretion of the Northern Arabian-Nubian shield: integrated evidence from central Eastern Desert Egypt.* Precambrian Research, 2022. **371**: p. 106599.
50. Gharib, M.E., et al., *Evolution of a Neoproterozoic island arc in the northern Arabian-Nubian Shield: Volcanic rocks and their plutonic equivalents in the Hamash area, south Eastern Desert, Egypt.* Precambrian Research, 2021. **358**: p. 106145.
51. Kröner, A., *Ophiolites and the evolution of tectonic boundaries in the late proterozoic Arabian—Nubian shield of northeast Africa and Arabia.* Precambrian Research, 1985. **27**(1): p. 277-300.
52. Kröner, A., *Pan-African mobile belts as evidence for a transitional tectonic regime from intraplate orogeny to plate margin orogeny*, in *Evolution and Mineralization of the Arabian–Nubian Shield*, A.M.S. Al-Shanti, Editor. 1979, Pergamon. p. 21-37.
53. Rogers, J.J.W., et al., *Plutonism in Pan-African belts and the geologic evolution of northeastern Africa.* Earth and Planetary Science Letters, 1978. **39**(1): p. 109-117.
54. Gérard, B., et al., *Impact of Inherited Foreland Relief on Retro-Foreland Basin Architecture.* Journal of Geophysical Research: Solid Earth, 2023. **128**(3): p. e2022JB024967.
55. Botziolis, C., et al., *Orogenic exhumation, erosion, and sedimentation in a pro-foreland basin: central Pindos foreland basin, western Greece.* Arabian Journal of Geosciences, 2023. **16**(8): p. 471.
56. Gérard, B., et al., *Impact of inherited geometries on syn-orogenic foreland basin*. 2022.
57. Sun, X., et al., *Fluvial sedimentation and its reservoir potential at foreland basin margins: A case study of the Puig-reig anticline (South-eastern Pyrenees).* Sedimentary Geology, 2021.

424: p. 105993.
58. Nagel, S., et al., *Sedimentology and foreland basin paleogeography during Taiwan arc continent collision.* Journal of Asian Earth Sciences, 2013. **62**: p. 180-204.
59. Sinclair, H., *Thrust Wedge/Foreland Basin Systems*, in *Tectonics of Sedimentary Basins*. 2011. p. 522-537.
60. DeCelles, P.G., *Foreland Basin Systems Revisited: Variations in Response to Tectonic Settings*, in *Tectonics of Sedimentary Basins*. 2011. p. 405-426.
61. Wuellner, D.E., L.R. Lehtonen, and W.C. James, *Sedimentary-Tectonic Development of the Marathon and Val Verde Basins, West Texas, U.S.A.: A Permo–Carboniferous Migrating Foredeep*, in *Foreland Basins*. 1986. p. 347-368.
62. Tankard, A.J., *On the Depositional Response to Thrusting and Lithospheric Flexure: Examples from the Appalachian and Rocky Mountain Basins*, in *Foreland Basins*. 1986. p. 369-392.
63. Sayed, S.M., et al., *Remote Sensing and Geological Characterization of the Polydeformed Atud Basin and Surrounding Rocks, Eastern Desert, Egypt.* Journal of African Earth Sciences, 2025. **(Under review)**.
64. Stern, R.J., et al., *The Atud gabbro–diorite complex: glimpse of the Cryogenian mixing, assimilation, storage and homogenization zone beneath the Eastern Desert of Egypt.* Journal of the Geological Society, 2020. **177**(5): p. 965-980.
65. Ali, K.A., et al., *U–Pb zircon geochronology and Hf–Nd isotopic systematics of Wadi Beitan granitoid gneisses, South Eastern Desert, Egypt.* Gondwana Research, 2015. **27**(2): p. 811-824.
66. Camp, V., *Island arcs and their role in the evolution of the western Arabian Shield.* Geological Society of America Bulletin - GEOL SOC AMER BULL, 1984. **95**.
67. Abdelsalam, M. and B. Stern, *Tectonic evolution of the Nakasib suture, Red Sea Hills, Sudan: evidence for a late Precambrian Wilson Cycle.* Journal of The Geological Society - J GEOL SOC, 1993. **150**: p. 393-404.
68. Dixon, T.H., *Age and chemical characteristics of some pre-Pan-African rocks in the Egyptian Shield.* Precambrian Research, 1981. **14**(2): p. 119-133.
69. Abdelsalam, M.G., et al., *Neoproterozoic deformation in the northeastern part of the Saharan Metacraton, northern Sudan.* Precambrian Research, 2003. **123**(2): p. 203-221.
70. Johnson, P.R., et al., *Late Cryogenian–Ediacaran history of the Arabian–Nubian Shield: A review of depositional, plutonic, structural, and tectonic events in the closing stages of the northern East African Orogen.* Journal of African Earth Sciences, 2011. **61**(3): p. 167-232.
71. Meinhold, G., et al., *Detrital zircon provenance of north Gondwana Palaeozoic sandstones from Saudi Arabia.* Geological Magazine, 2020. **158**(3): p. 442-458.
72. Li, Z.-X., D.A.D. Evans, and G.P. Halverson, *Neoproterozoic glaciations in a revised global palaeogeography from the breakup of Rodinia to the assembly of Gondwanaland.* Sedimentary geology, 2013. **294**: p. 219-232.
73. Hood, A.v.S., et al., *Neoproterozoic syn-glacial carbonate precipitation and implications for a snowball Earth.* Geobiology, 2022. **20**(2): p. 175-193.
74. Yu, W., et al., *Cryogenian cap carbonate models: a review and critical assessment.* Palaeogeography, Palaeoclimatology, Palaeoecology, 2020. **552**: p. 109727.
75. Abd El-Rahman, Y., et al., *Not all Neoproterozoic iron formations are glaciogenic: Sturtian-aged non-Rapitan exhalative iron formations from the Arabian–Nubian Shield.* Mineralium Deposita, 2020. **55**(3): p. 577-596.
76. Lei, R.-X., et al., *Neoproterozoic non-glaciogenic iron formation: Insights from Fe isotope and elemental geochemistry of the Shalong iron formation from the Central Tianshan block, southern Altaids.* Precambrian Research, 2020. **351**: p. 105959.
77. Basta, F.F., et al., *Petrology and geochemistry of the banded iron formation (BIF) of Wadi Karim and Um Anab, Eastern Desert, Egypt: Implications for the origin of Neoproterozoic BIF.* Precambrian Research, 2011. **187**(3): p. 277-292.
78. Beyth, M., et al., *Crustal exhumation and indications for Snowball Earth in the East African Orogen: north Ethiopia and east Eritrea.* Precambrian Research, 2003. **123**(2): p. 187-201.
79. Kennedy, M.J., N. Christie-Blick, and A.R. Prave, *Carbon isotopic composition of Neoproterozoic glacial carbonates as a test of paleoceanographic models for snowball Earth*

phenomena. Geology, 2001. **29**(12): p. 1135-1138.
80. James, N.P., G.M. Narbonne, and T. Kurtis Kyser, *Late Neoproterozoic cap carbonates: Mackenzie Mountains, northwestern Canada: precipitation and global glacial meltdown.* Canadian Journal of Earth Sciences, 2001. **38**(8): p. 1229-1262.
81. Sayed, S.M., et al., *Is the Neoproterozoic Atud diamictite of glacial or non-glacial origin in the Eastern Desert, Egypt? Evidence from field observations and remote sensing images*, in *1st International Science Conference*. 2023: Helwan University.
82. Lowe, D.R. and G.R. Byerly, *The non-glacial and non-cratonic origin of an early Archean felsic volcaniclastic unit, Barberton Greenstone Belt, South Africa.* Precambrian Research, 2020. **341**: p. 105647.
83. Dowdeswell, J.A., L.E. Osterman, and J.T. Andrews, *Quartz sand grain shape and other criteria used to distinguish glacial and non-glacial events in a marine core from Frobisher Bay, Baffin Island, N.W.T., Canada.* Sedimentology, 1985. **32**: p. 119-132.
84. Visser, J.N.J., *Submarine debris flow deposits from the Upper Carboniferous Dwyka Tillite Formation in the Kalahari Basin, South Africa.* Sedimentology, 1983. **30**(4): p. 511-523.
85. Kosun, E., et al., *Syn-tectonic sedimentary evolution of the Miocene Çatallar Basin, southwestern Turkey.* Journal of Asian Earth Sciences, 2009. **34**(3): p. 466-479.
86. Swanson-Hysell, N.L., et al., *Stratigraphy and geochronology of the Tambien Group, Ethiopia: Evidence for globally synchronous carbon isotope change in the Neoproterozoic.* Geology, 2015. **43**(4): p. 323-326.
87. Park, Y., et al., *The lead-up to the Sturtian Snowball Earth: Neoproterozoic chemostratigraphy time-calibrated by the Tambien Group of Ethiopia.* Bulletin, 2020. **132**(5-6): p. 1119-1149.
88. Guisado, R., I. Armenteros, and C. Dabrio, *Sedimentación continental paleógena entre Almazul y Deza (Cuenca de Almazán Oriental, Soria).* Studia geologica salmanticensia, ISSN 0211-8327, Vol. 25, 1988, pags. 67-85, 1988.
89. Lopes, G., et al., *Provenance of the reworked Ordovician Palynomorphs in SDJ1 Borehole - Santa Susana Basin, Ossa Morena Zone, Portugal*. 2012.
90. Powell, J., A. Abed, and Y.-M. Nindre, *Cambrian stratigraphy of Jordan.* GeoArabia, 2014. **19**.
91. Sehsah, H., et al., *Evolution of the Neoproterozoic Kareim Basin, north Arabian – Nubian shield.* Scientific Reports, 2025. **15**(1): p. 17534.
92. Fowler, A., et al., *Remote sensing-guided stratigraphic dissection of an Ediacaran terrestrial molasse basin (Kareim basin, Egypt), with implications for sedimentary evolution.* Precambrian Research, 2020. **338**: p. 105589.